〈일반논문〉
Journal of the Korean Society of Visualization, Vol. 19, No. 3 (69~76), 2021
(Manuscript received : 2021.10.12./Revised : 2021.11.18./Accepted : 2021.12.03.)
DOI:http://dx.doi.org/10.5407/jksv.2021.19.3.069

ISSN 1598-8430 Print
ISSN 2093-808X Online

Design of sinusoidal shape channel PCHEs for supercritical LNG based on CFD simulation

Jinxing Fan* and Eunseop Yeom†

CFD 시뮬레이션 기반 초임계 LNG용 사인함수 PCHE 설계

판진싱* · 염은섭†

Abstract Printed circuit heat exchanger (PCHE) is a compact heat exchanger with good heat transfer performance, high structure integrity, and reliability over a wide range of temperatures and pressures. Instead of the traditional zigzag and straight shape channel, the sinusoidal shape channel was adopted in this study to investigate the relation of thermal-hydraulic performance and waviness factors (period and amplitude). The local flow characteristics and the heat flux distribution were compared to verify the effects of period and amplitude on heat transfer performance. As the period of channel becomes shorter, the rapid change of the flow direction can produce high flow separation around the corner leading to the disturbance of the boundary layer opposite wall. The nonuniform distribution of flow velocity appeared around the corner positions can promote fluid mixing and lead to higher thermal performance. An evaluation index was used to compare the comprehensive performance of PCHE considering the Nusselt number and Fanning factor. Based on the simulation results, the optimal design parameters of PCHE channel shape were found that the channel with an equivalent bending angle of 15° offers the highest heat flux capacity.

Key Words : Printed circuit heat exchanger(인쇄형 열교환기), Sinusoidal waviness(사인 함수 채널), Heat flux(열유속), Liquefied natural gas(액화 천연 가스)

1. Introduction

The printed circuit heat exchanger (PCHE) consists of many microchannels by using the photo-chemical etching technique and diffusion bonding method. The microchannel structure reduces the heat exchanger volume and provides a large heat transfer area which can achieve higher heat transfer performance. In addition, the diffusion bonding technique ensures the PCHE can show high reliability performance over a wide range of temperatures and pressures.(1) PCHEs have been widely applied in the new generation of nuclear power, floating liquefied natural gas devices, Brayton-cycle heat exchangers due to a series of advantages: high heat transfer ability, compact size, and high reliability.(2-5) With the increasing demand for LNG technology, the lightness, compactness, and

† School of Mechanical Engineering, Pusan National University (PNU), Associate Professor
E-mail: esyeom@pusan.ac.kr
* School of Mechanical Engineering, PNU, MS student.

reliability of PCHEs have been highlighted as a piece of promising equipment.[6]

Thermal-hydraulic performance shows different responses to the effect of physical influence factors. In straight shape channel, the flow characteristics along the flow direction can be clearly observed due to the simplified structure.[7-8] To reach a better heat transfer performance, the zigzag shape channel was adopted to increase heat transfer area as well as compact the volume compared with the straight shape channel.[9] While the flow separation appears near the bending corners, the round corner zigzag shape channel and wavy shape channel were introduced to reduce pressure drop near the bending corners.[2-3] The previous research results show that the round corner structure can evidently inhabit the flow separation and then reduce the pressure drop. In addition, the optimization bending angle was investigated and the best performance was found at an angle of 15°.[10]

According to our previous study about supercritical-LNG PCHEs, the sinusoidal shape channel with an equivalent bending angle of 15° showed a better thermal-hydraulic performance compared with the zigzag shape channels.[11] Since sinusoidal shape is defined by combination of period and amplitude, the flow characteristics, the heat flux distribution of corresponded area is also discussed to study the fluid accelerate effect induced by waviness effect at a constant mass flow rate of 2.0×10^{-4} kg/s. Three cases with same channel surface area are used to explain the waviness effect of heat transfer performance. And the average heat flux of different equivalent bending angle is compared to verify the previous research result of the bending angle effect.

2. Numerical model and solution method

2.1 Physical model and boundary condition

Fig. 1 shows a diagram of the model. The cross-section structure and boundary conditions are

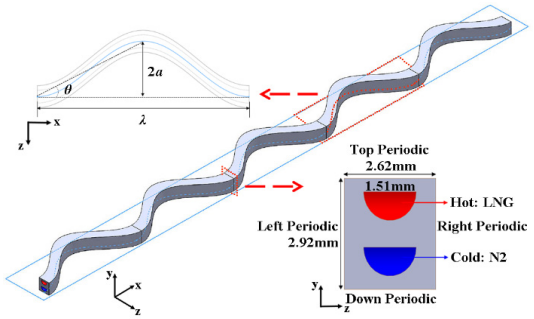

Fig. 1. Diagrams of PCHE with sinusoidal channel.

Table 1. Geometric features of sinusoidal channels.

Case	Period λ (mm)	Amplitude a (mm)	Area (mm^2)	Equivalent bending angle θ
1	12.3	0.825	1.93×10^3	15°
2	12.3	1.65	2.00×10^3	28°
3	12.3	3.3	2.23×10^3	47°
4	24.6	0.825	1.91×10^3	8°
5	24.6	1.65	1.93×10^3	15°
6	24.6	3.3	2.00×10^3	28°
7	49.2	0.825	1.91×10^3	4°
8	49.2	1.65	1.91×10^3	8°
9	49.2	3.3	1.93×10^3	15°

same as our previous research.[11] The two waviness factors including the amplitude (a) and the period (λ) are defined as 0.825, 1.65, 3.3 mm and 12.3, 24.6, 49.2 mm, respectively. In addition, the 492mm of full-length channel (L) consists of 40, 20, 10 pitches depending on the period. Detail parameters of each case are summarized in Table 1.

The inlet and outlet boundaries of the fluid were set as mass flow inlet and pressure outlet, respectively. Supercritical LNG (340 K) and liquid nitrogen (121 K) flow in opposite directions as hot and cold working fluids with the same mass flow rate of 2.0×10^{-4} kg/s. The solid was composed of SS316L with a density of 8000 kg/m^3, specific heat of 535 J/kg·K, and thermal conductivity of 14.6 W/m·K. It was assumed that SS316L's properties do not change with temperature. The thermal physical properties of

supercritical LNG were obtained from NIST-REFPROP software in a range of temperature from 100 K to 400 K at 10.5 MPa.

2.2 Grid independence study

The boundary layer options were same as our previous study of zigzag shape channel PCHEs. A preliminary grid independence study for the model of case 5 was carried out.[11] When the gird number was greater than 3.1 million, the relative deviations of average outlet temperature and pressure drop are less than 0.5%.

2.3 Computational method

The commercial software ANSYS Fluent 2020 R2 was selected as the tool for the numerical simulation. The SIMPLEC algorithm was selected to couple the pressure and velocity. For the stable algorithm and high accuracy near the wall in supercritical fluid region, shear stress transport k-ω turbulence model was used.[2] All equations were solved by the second-order upwind discretization scheme. The criterion for convergence was that the monitored parameters (k, ω, and momentum) of the inlet and outlet should be steady.

In this study, the phase change process is not considered based on the previous study comparing the results depending on the phase change.[12] The effect of axial conduction is negligible compared with convection heat transfer between fluid and channels when the Reynolds number is bigger than 1250.[13] The average Reynolds number in this study is bigger than 8540, which is the turbulent flow region.

The following governing equations of continuity, momentum, and energy were used in the calculation:
Continuity equation:

$$\frac{\partial}{\partial x_i}(\rho u_i) = 0 \tag{1}$$

where ρ is the density, and u_i is the velocity vector
Momentum equation:

$$\frac{\partial}{\partial x_j}(\rho u_i u_j) = -\frac{\partial P}{\partial x_i} + \rho g_i + \frac{\partial}{\partial x_j}\left[(\mu + \mu_t)\frac{\partial u_i}{\partial x_j}\right] \tag{2}$$

where P is the pressure, and μ and μ_t are the dynamic and turbulent viscosities, respectively.
Energy equation:

$$\frac{\partial}{\partial x_i}(u_i(\rho H + P)) = \frac{\partial}{\partial x_i}\left(\lambda_{eff}\frac{\partial T}{\partial x_i} + u_i \tau_{ij}\right) \tag{3}$$

where λ_{eff} is the effective conductivity, H is the specific enthalpy, and τ_{ij} is the Reynolds stress.

The transport equations for shear stress transport k-ω model are:

$$\frac{\partial}{\partial x_i}(\rho k u_i) = \frac{\partial}{\partial x_j}\left[(\mu + \frac{\mu_t}{\sigma_k})\frac{\partial k}{\partial x_j}\right] + G_k - Y_k \tag{4}$$

$$\frac{\partial}{\partial x_i}(\rho \omega u_i) = \frac{\partial}{\partial x_j}\left[(\mu + \frac{\mu_t}{\sigma_\omega})\frac{\partial \omega}{\partial x_j}\right] + G_\omega - Y_\omega + D_\omega \tag{5}$$

where the Prandtl numbers for k and ω are $\sigma_{k,1}$ = 1.176, $\sigma_{k,2}$ = 1.0, and $\sigma_{\omega,1}$ = 2.0, $\sigma_{\omega,2}$ = 1.168. Detailed information of G_k, Y_k, G_ω, Y_ω, and D_ω can be found in a reference.[14]

The Reynolds number, Nusselt number, Fanning factor and Dean number are defined as:

$$Re = \frac{\rho v D_h}{\mu} \tag{6}$$

$$Nu = \frac{hD_h}{\bar{\lambda}} = \frac{qD_h}{\bar{\lambda}(T_b - T_s)} \tag{7}$$

$$f = \frac{\Delta P D_h}{2L\rho v^2} = \frac{\Delta P D_h \rho A_c^2}{2L\dot{m}^2} \tag{8}$$

$$De = Re\sqrt{\frac{D_h}{2R_c}} \tag{9}$$

where v is the fluid velocity, D_h is the hydraulic diameter. h, $\overline{\lambda}$ and q are the heat transfer coefficient, average thermal conductivity, and surface heat flux. T_b and T_s are the bulk mean temperature and surface mean temperature, respectively. L is the channel path length, and A_c is the cross-section area of the channel. R_c is the radius of curvature of the corner area.

3. Numerical results and discussion

In this study, the effects of the channel waviness factors on the thermal-hydraulic performance were investigated varying with the period and periodic. Nine cases of different period and amplitude with the same hydraulic diameter were adopted. The heat transfer performance was compared at a constant mass flow rate of 2.0×10^{-4} kg/s.

3.1 Flow characteristics and heat flux

The local flow characteristics are fundamental to understand the heat transfer performance of different channel shape PCHEs. Fig. 2 shows the hot channel local velocity distribution at a pitch of middle length of case 1, 5, and 9 with same equivalent bending angle ($\theta = 15°$) considering previous recommendation.[10,11] Similar to previous result, the bending corner produces a change in the flow direction skewed to the outer wall of bending.[11] Five cross sections were extracted from the each pitch. The specific positions are shown in Table 2. At cross sections of B and D, the skewed flow (right for B and left for D) has no secondary flow with higher average velocity. At bending corner (A, C and E), the significant secondary flows are observed with large Dean vortex structures induced by the centrifugal force. The corner area Dean number of three cases are 43, 60 and 85, respectively. The result shows the Dean number increase with the period and the long period structures contribute to a stable vortex. There are two differences of the Dean vortex structure from the

Table 2. Specific positions of cross sections.

Cross section	Position
A	$\frac{L}{2}-\frac{\lambda}{2}$
B	$\frac{L}{2}-\frac{\lambda}{4}$
C	$\frac{L}{2}$
D	$\frac{L}{2}+\frac{\lambda}{4}$
E	$\frac{L}{2}+\frac{\lambda}{2}$

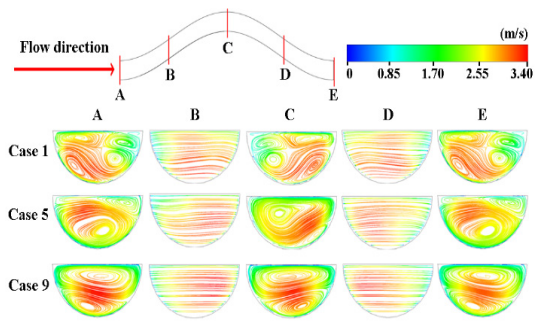

Fig. 2. Velocity distribution at different cross-section.

Fig. 2. The first one is the quantity of vortexes, it can be seen that there are 4 vortexes in case 1, only 2 vortexes in case 5 and case 9. The second one is the center position of the vortexes, the vortexes of case 1, and case 5 are skewed to the edge position, while the vortexes of case 9 are almost in the middle of the cross section. The differences can be explained by the channel structure, the shortest period is in case 1 which can force the fluid change the flow direction rapidly with high frequency compared with case 5 and case 9. And the longest period is in case 9 which made the channel structure is close to straight channel, the high velocity core of the fluid stays in the middle of the channel and move within a short distance. From the flow characteristics it can be deduced that complex secondary flows promote efficient cross-sectional fluid mixing and enhance the heat transfer rate significantly by comparing with heat flux distribution.

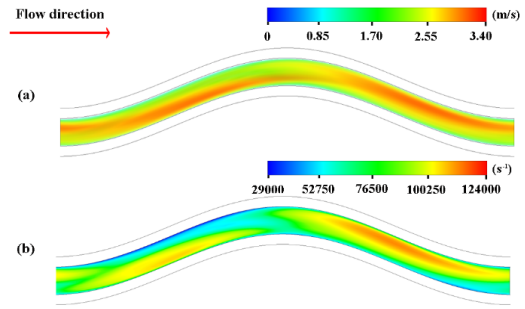

Fig. 3. Streamwise (a)velocity and (b) vorticity of case 5.

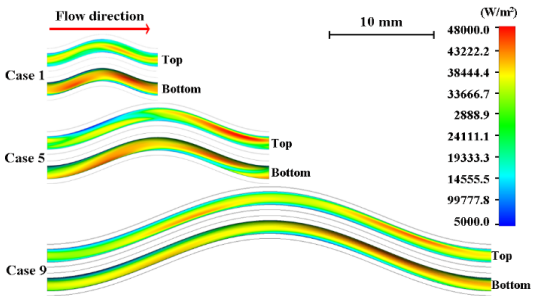

Fig. 4. Heat flux distribution at top and bottom of channel.

Fig. 3a shows the local velocity distribution along the flow direction of the middle pitch of case 5. The flow separation induced by the centrifugal force can be observed around the corner area. Fig. 3b shows the vorticity of the same position. It can be found that higher velocity gradient appears at position of B and D which correspond the cross-section velocity distribution in Fig. 2. This is because the accelerate effect after changing flow direction. The high velocity fluid impact at the channel surface which can disturb the boundary layer.

The heat flux distributions at top and bottom of channel are shown in Fig. 4. The higher heat flux was observed after passing the banding corner around cross section B and D. This can be explained by the centrifugal force after passing the corner disturbs the boundary layer with a higher velocity. Complex secondary flows for case 1 produce relatively uniform heat flux at bottom. The wider region with high velocity near the channel top surface for case 5, lead to the higher heat flux at the corresponding area.

The cross-section velocity distribution form Fig. 2 also indicate the temperature distribution, high velocity area matched well with the high temperature area because the heat transfer time is not sufficient in the flow region with the high velocity. According to the thermal physical properties of supercritical LNG, the density and viscosity increase with the temperature decreases. The Fanning factor is proportional to pressure drop and density, led to the higher Fanning factor near the edge position than other area. The difference of friction factor enhances the Dean vortex when the fluid change flow direction. In addition, the enhanced Dean vortex structure is contributed to the fluid mixing as well as heat transfer performance.

3.2 Average heat flux of different waviness factors

For depicting the relation between flow characteristics and heat transfer depending on channel shape, the result of case 1, 5, and 9 with the same heat transfer area were compared in previous section. As for other cases, the heat transfer area is proportional to the amplitude, period, and pitch number. For a fair comparison of heat transfer performance, the average heat flux ($\bar{q}$) is plotted in Fig. 5. As a comparison, the straight shape channel's average heat flux is also inserted in Fig. 5 (amplitude = 0). According to the simulation result, case 1 shows the highest average heat flux. The channel with an equivalent angle of 15° (case 1, 5, 9) can produce a higher average heat flux among the equivalent amplitude. The simulation result verified that our previous research that sinusoidal shape channel PCHE with an equivalent bending angle of 15° can produce the best heat transfer performance. Even though case 1, 5, 9 have the same heat transfer area, the average heat flux is not same which are 44,327 W/m^2, 43,587 W/m^2, and

43,200 W/m^2. This can be explained by the enhancement of turbulence induced by the change of the flow direction in the small period, which varies with the waviness factors (Fig. 2). As the channel structure is close to the straight channel (case 4, 7, 8), the average heat flux gradually converges to a value of straight channel (43,249 W/m^2).

In case of 3.3 mm amplitude, the significant flow disturbance caused by high bending angle produced lower average heat flux compared to the straight's value. Case 3 shows smallest average heat flux among cases.

In our preliminary test changing mass flow rate from 1.0×10^{-4} kg/s to 5.0×10^{-4} kg/s for case 5, the average heat flux is proportional to the mass flow rate. Heat transfer performance caused by the flow characteristic may be not dramatically varied depending on the mass flow rate in the range of 1.0- 5.0×10^{-4} kg/s.

3.3 Comprehensive performance of different waviness factors

The average heat flux can only reflect the heat transfer capacity. Another important factor: Fanning factor of PCHE should also be considered to estimate the comprehensive performance of the full channel. The evaluation index $\xi = (\overline{Nu}\,/Nu_o)/(\bar{f}\,/f_o)$ is quoted to reflect the thermal-hydraulic performance of PCHEs, which is consist of the average Nusselt number ($\overline{Nu}$), average Fanning factor ($\bar{f}$), Nusselt number of channel outlet (Nu_o) and Fanning factor of channel outlet (f_o).[10] Fig. 6 shows the evaluation index of different channel waviness factors. Case 3 has a relativity high evaluation index among the PCHE configurations. This is because case 3 has the biggest channel surface which led to the highest heat transfer rate. Even though the channel with the equivalent bending angle of 15° can produce the highest average heat flux, when the heat transfer area is considered, the effect of increased heat transfer area on thermal-hydraulic performance is dominant factors.

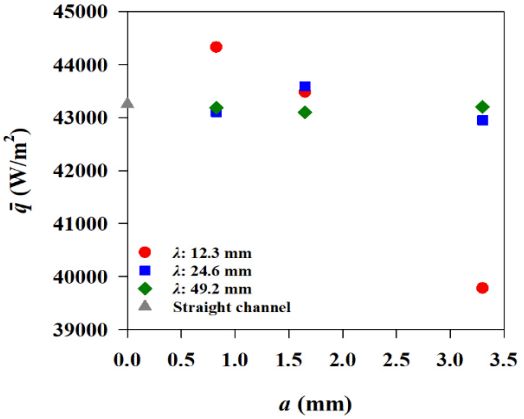

Fig. 5. Average heat flux of different waviness factors.

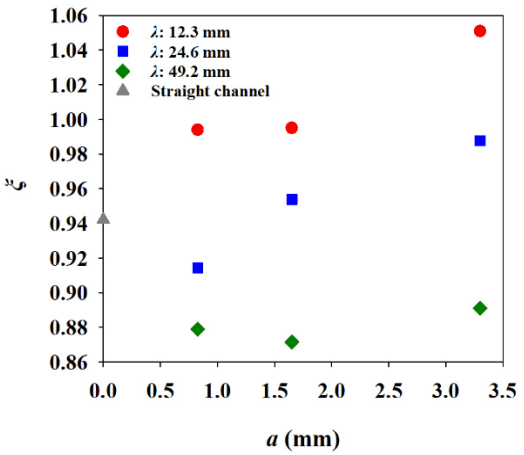

Fig. 6. Evaluation index value ξ of different waviness

4. Conclusions

In this paper, three-dimensional numerical model of different waviness factors is established to investigate the optimal thermal-hydraulic performance design. The flow characteristics, heat transfer rate, and comprehensive performance were discussed to find the relations between waviness factors and thermal-hydraulic performance. Based on the numerical results, the following conclusions are derived.

(1) The high velocity areas near the channel surface correspond well with the high heat flux areas which can be explained by the disturbance of the boundary layer.

(2) Whether in the same period or same amplitude, the channel with an equivalent angle of 15° can produce a higher average heat flux among the equivalent bending angle configurations. As for the comprehensive performance of the full channel, the highest evaluation index can be found at the biggest heat transfer area channel (Case 3).

(3) According to the simulation results, the effect of turbulence is conducive to heat transfer capacity. And the turbulence effect in the channel with an equivalent bending angle of 15° produces the optimization solution of the heat transfer performance. While for the full channel, the bigger heat transfer area is more conducive to the comprehensive performance.

Acknowledgments

This work was supported by the National Research Foundation of Korea(NRF) grant funded by the Korea government(MSIT) (No. 2021R1I1A3047664).

REFERENCE

1) Takeda T., Kunitomi K., Horie T., and Iwata K., 1997, “Feasibility study on the applicability of a diffusion-welded compact intermediate heat exchanger to next-generation high temperature gas-cooled reactor,” Nuclear engineering and design, Vol. 168 (1-3), pp. 11-21.

2) Bai J., Pan J., He X., Wang K., Tang L., and Yang R., 2020, “Numerical investigation on thermal hydraulic performance of supercritical LNG in sinusoidal wavy channel based printed circuit vaporizer,” Applied Thermal Engineering, Vol. 175, pp. 115379.

3) Baik S., Kim S. G., Lee J., and Lee J. I., 2017, “Study on CO_2-water printed circuit heat exchanger performance operating under various CO_2 phases for S-CO_2 power cycle application,” Applied Thermal Engineering, Vol. 113, pp. 1536-1546.

4) Hinze J. F., Nellis G. F., and Anderson M. H., 2017, “Cost comparison of printed circuit heat exchanger to low cost periodic flow regenerator for use as recuperator in a s-CO2 Brayton cycle,” Applied energy, Vol. 208, pp. 1150-1161.

5) Kim I. H., and No H. C., 2013, “Thermal-hydraulic physical models for a printed circuit heat exchanger covering He, He-CO_2 mixture, and water fluids using experimental data and CFD,” Experimental thermal and fluid science, Vol. 48, pp. 213-221.

6) Barclay M., and Denton N., 2005, “Selecting offshore LNG processes.” LNG journal, Vol. 10 (1), pp. 34-36.

7) Aneesh A., Sharma A., Srivastava A., Vyas K., and Chaudhuri P., 2016, “Thermal-hydraulic characteristics and performance of 3D straight channel based printed circuit heat exchanger,” Applied Thermal Engineering, Vol. 98, pp. 474-482.

8) Xu H., Duan C., Ding H., Li W., Zhang Y., Hong G., and Gong H., 2021, “The optimization for the straight-channel PCHE size for supercritical CO2 Brayton cycle,” Nuclear Engineering and Technology, Vol. 53 (6), pp. 1786-1795.

9) Kim I. H., and No H. C., 2012, “Physical model development and optimal design of PCHE for intermediate heat exchangers in HTGRs,” Nuclear Engineering and Design, Vol. 243, pp. 243-250.

10) Pan J., Wang J., Tang L., Bai J., Li R., Lu Y., and Wu G., 2020, “Numerical investigation on thermal-hydraulic performance of a printed circuit LNG vaporizer,” Applied Thermal Engineering, Vol. 165, pp. 114447.

11) Fan J., and Yeom E., 2022, “Numerical investigation on thermal hydraulic performance of supercritical LNG in PCHEs with straight, zigzag, and sinusoidal channels,” Journal of Visualization, in press.

12) Zhang P., Ma T., Ke H., Wang W., Lin Y., and Wang Q., 2019, “Numerical investigation on local

thermal characteristics of printed circuit heat exchanger for natural gas liquefication," Energy Procedia, Vol. 158, pp. 5408-5413.
13) Tang L. H., Yang B. H., Pan J., and Sundén B., 2021, "Thermal performance analysis in a zigzag channel printed circuit heat exchanger under different conditions," Heat Transfer Engineering.
14) Menter F. R., 1994, "Two-equation eddy-viscosity turbulence models for engineering applications," AIAA journal, Vol. 32 (8), pp. 1598-1605.